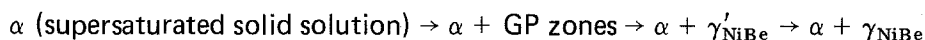


# Precipitation in a nickel-beryllium alloy

T. V. NORDSTROM, C. R. HILLS

*Sandia Laboratories, Albuquerque, New Mexico 87115, USA*

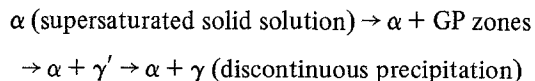
Precipitation was studied in a nickel 1.89 wt % beryllium alloy over the temperature range 400 to 750° C. Below 650° C, the precipitation sequence is analogous to that in the widely studied Cu–Be system:



where the equilibrium  $\gamma_{\text{NiBe}}$  phase is formed by a discontinuous reaction consuming the intermediate  $\gamma'_{\text{NiBe}}$ . The morphology of the discontinuous  $\gamma_{\text{NiBe}}$  was too irregular to assign a habit plane. Numerous orientation relations were observed between the  $\alpha_{\text{Ni}}$  and the discontinuous  $\gamma_{\text{NiBe}}$ . The kinetics of the reaction were found to follow a linear growth with time. The activation energy of  $58 \pm 3 \text{ kcal mol}^{-1}$  is less than bulk diffusion of nickel but greater than grain boundary self diffusion. Above 650° C, the discontinuous reaction front is arrested before completion because the equilibrium  $\gamma_{\text{NiBe}}$  forms by continuous coarsening of the  $\gamma'_{\text{NiBe}}$  phase. The continuous  $\gamma_{\text{NiBe}}$  has a habit plane of  $\{113\}_{\alpha}$ . Three closely related orientations were observed at constant ageing parameters for the equilibrium continuous phase. Each has been separately proposed in the literature as a unique relation for the copper–beryllium system. For nickel–beryllium either all three are uniquely present or the accuracy of selected area diffraction technique is such that the small differences in orientation cannot be distinguished.

## 1. Introduction

The nickel–beryllium system has been described as similar to the widely studied copper–beryllium system with respect to the sequence and structure of the precipitation phases on ageing [1]. While there is some disagreement in the literature, the precipitation sequence on ageing in copper–beryllium appears to be as follows [2–8]:



The  $\gamma'$  precipitate are ordered platelets nucleating on GP zones and coherent on  $\{100\}$  matrix planes. The semi-coherent  $\gamma'$  has a B2 superlattice and as it coarsens the habit plane rotates from the  $\{001\}_{\alpha}$  to the  $\{113\}_{\alpha}$ . The most commonly proposed orientation relations is  $(113)_{\alpha} \parallel (130)_{\gamma'}$ ;  $[110]_{\alpha} \parallel [001]_{\gamma'}$ . Equilibrium  $\gamma$  phase is formed by a discontinuous precipitation reaction that consumes the  $\gamma'$  phase and has essentially the same structure and lattice parameter as the  $\gamma'$  but a slightly

different orientation relation to the matrix [8].

The present work studied the kinetics, morphology and structure of the precipitation reactions in nickel–beryllium. No comprehensive studies of Ni–Be reaction kinetics or precipitate structure were found in the literature. It is known, however, that the intermediate phases are similar [1] to copper–beryllium and a discontinuous reaction does occur at temperatures well below the solvus [9].

## 2. Experimental procedure

The nickel–beryllium alloy was obtained in the form of 1 mm × 25 mm strip. The chemical composition is presented in Table I. Common designation for the material is nickel–beryllium alloy 440. Samples were vacuum-annealed for 30 min at 1000° C and water quenched. Ageings were performed in forming gas (93% N<sub>2</sub>, 7% H<sub>2</sub>) at 400, 465, 510, 565, 650 and 750° C. Ageing times ranged from 5 min to 1000 h.

TABLE I Composition of nickel–beryllium alloy (wt%)

Be	Fe	Si	Al	B	C	Pb	Ti	Cr	Mg	Ni
1.89	0.12	0.03	0.03	<0.001	0.027	0.001	0.47	0.06	0.003	Balance

The kinetics of the discontinuous precipitation reactions were studied using quantitative optical metallography. Measurements of the fraction of area of the transformed regions were made on sectioned, polished and etched samples using the Imanco Quantimet 7000 system. Regions containing approximately 400 grains were measured for each ageing time and temperature in order to achieve a statistically significant measure of the fraction of area transformed.

Transmission electron microscopy was used to determine the morphology in the continuous and discontinuous reaction regions. Selected area electron diffraction was also employed to determine orientation relations between the matrix and precipitate phases.

### 3. Results and discussion

#### 3.1. Intermediate precipitation

The precipitation sequence was followed using electron diffraction. Fig. 1 shows a series of  $[110]_{\alpha}$  matrix patterns for three ageing times at  $565^{\circ}\text{C}$ . After 15 min there is streaking and the onset of intensity maxima [9]. This corresponds to a mixed structure of GP zones and the  $\gamma'$  phase. The GP zones are parallel to  $\{100\}_{\alpha}$ . With further ageing the intensity maxima broadens and after four hours becomes a triangular spot. The edges of the triangular spot are parallel to  $\{113\}_{\alpha}$ . Identical observations have been made in copper–beryllium [8]. The broadening corresponds to coarsening of the  $\gamma'$  and rotation of the habit plane from  $\{100\}_{\alpha}$  to  $\{113\}_{\alpha}$ . Thus the intermediate phase reactions

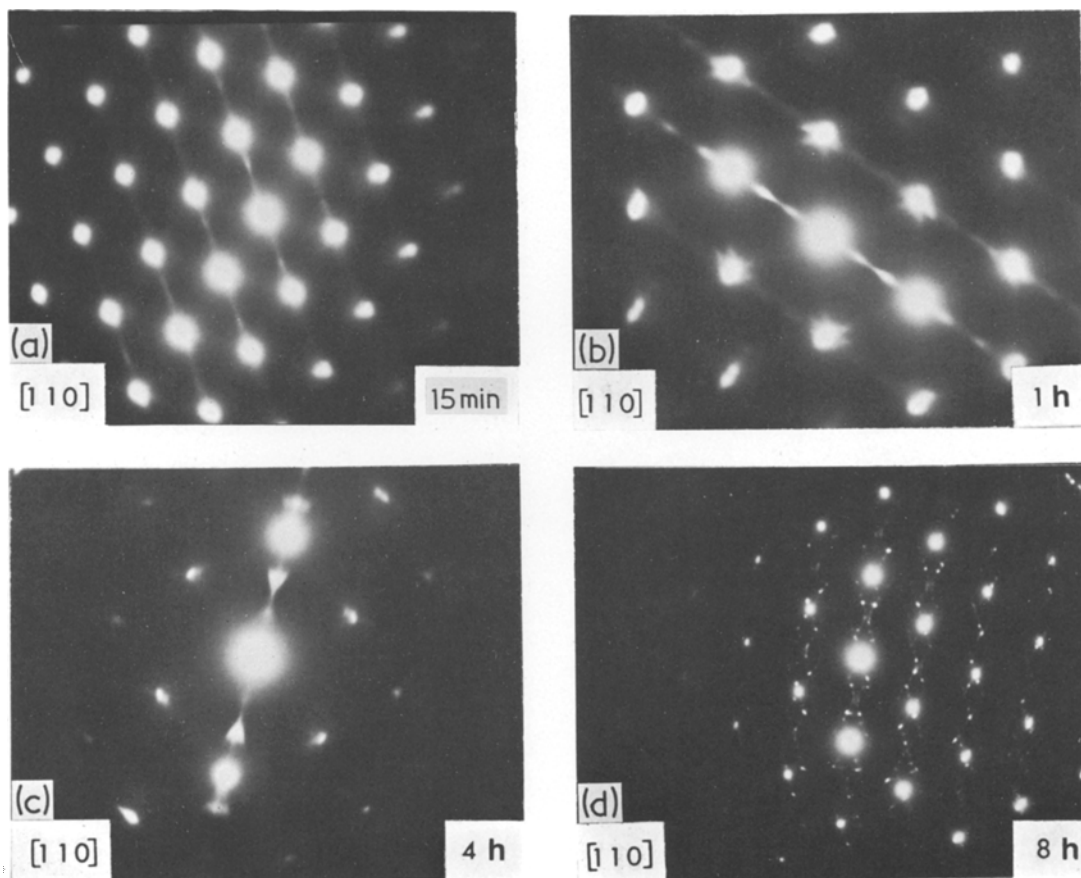


Figure 1 Selected area diffraction patterns for samples ages (a) 15 minutes, (b) 1 hour and (c) 4 hours at  $565^{\circ}\text{C}$ .  $[110]_{\alpha}$  pattern.

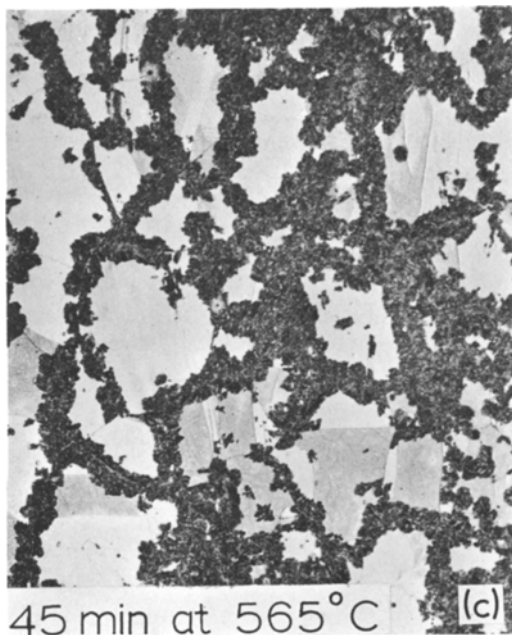
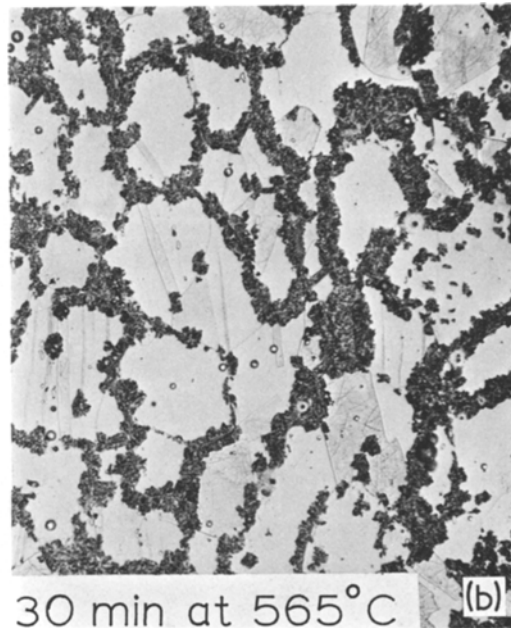
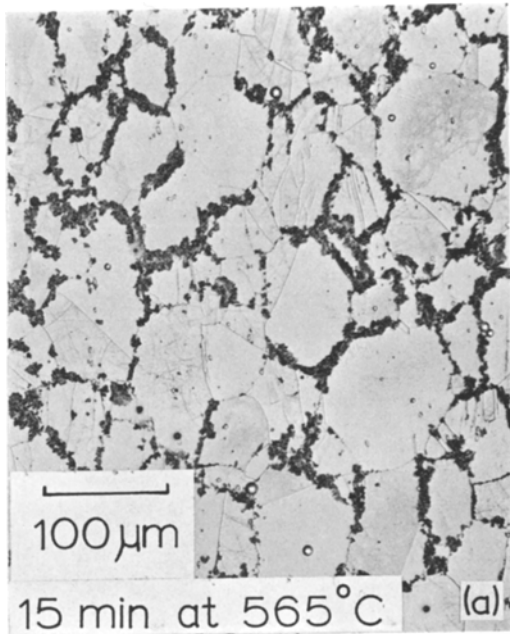


Figure 2 Optical photomicrographs showing successive stages in discontinuous precipitation reaction.

are identical in structure to copper–beryllium. The two means of transformation to the equilibrium  $\gamma$  will be presented in the following sections.

### 3.2. Optical metallography

Fig. 2 shows a series of optical micrographs for samples aged for various times at 565°C. The great contrast between the reacted and unreacted regions facilitated the use of quantitative metallography to measure the average extent of the trans-

formation. The discontinuous reaction is progressing from the grain boundaries. Transmission electron microscopy revealed regions of discontinuous reaction product adjacent to most boundaries, even for short ageing times. Also, the rates of reaction vary from boundary to boundary. Gruhl and Ammanns showed a strong dependence of growth rate on grain boundary misorientation in copper–beryllium [10]. Cahn analysed these results in terms of differences in boundary diffusion rate with misorientation [11].

Results of the quantitative metallography are shown in Fig. 3. Generally the transformation rates are linear up to about 75% transformed, as is predicted for discontinuous type reactions [12]. Above this amount of transformation, the rate falls below the linear rate due to impingement of colonies on each other, only large grains or more slowly growing cells still have unconsumed matrix available. Discontinuous precipitation can often be described by an equation for the transformation rate,  $\dot{f}$ , as

$$\dot{f} = K(\Delta T)^n \exp \frac{-Q}{kT}$$

where  $K$  is a constant,  $\Delta T$  is the undercooling below the solvus and  $Q$  is the activation energy for the diffusion process [13]. This equation assumes

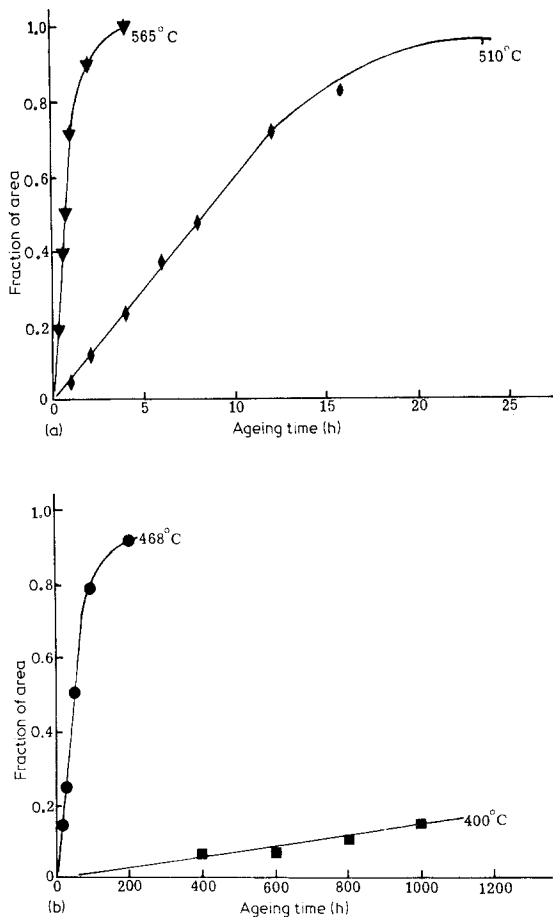


Figure 3 Fraction of area of discontinuously transformed versus ageing time for various ageing temperatures.

all nucleation has occurred at time zero. This assumption is verified by transmission electron microscopy on as-quenched samples which reveals numerous small colonies of the discontinuous precipitation already present. The equation predicts a maximum in  $f$  with temperature whereas Fig. 3 shows only a continuous increase in  $f$  with increasing temperature. In the present case, all the ageing temperatures are at least 200°C below the solvus temperature. Also, the semi-coherent  $\gamma'$  intermediate precipitate which is being consumed by the discontinuous reaction has a large amount of strain energy associated with it [14]. Both these conditions can contribute to the rate of reaction not showing a maximum with temperature. If the discontinuous reaction could be studied close to the solvus temperature, then perhaps a maximum in rate would be found. However, as will be shown later, at higher temperatures the discontinuous reaction is suppressed.

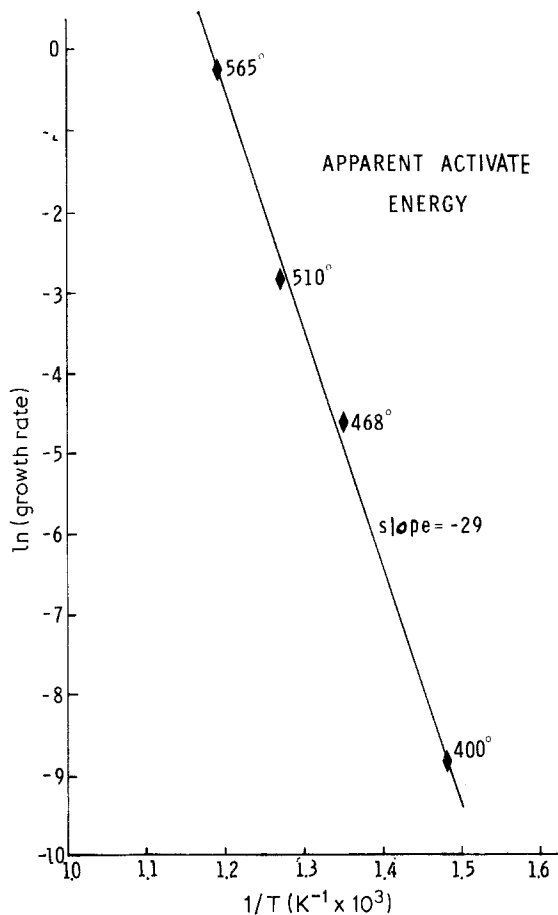


Figure 4 Determination of apparent activation energy from the measured temperature dependence of the transformation rate.

A reasonable estimate can be made for the activation energy for diffusion by plotting log transformation rate versus the reciprocal of absolute temperature and disregarding the undercooling term. Fig. 4 shows that over eight orders of magnitude the log transformation rate is linear with inverse temperature and corresponds to an activation energy of  $58 \pm 3 \text{ kcal mol}^{-1}$ . This is below the 67 to 70  $\text{kcal mol}^{-1}$  commonly observed for volume diffusion of nickel in nickel [15]. The pure nickel-in-nickel grain boundary diffusion activation energy is about 25  $\text{kcal mol}^{-1}$  [16]. No data is available for diffusion, either bulk or grain boundary of nickel in nickel-beryllium or of beryllium in nickel. However, work on grain boundary diffusion in some nickel alloys does show activation energies of about 50  $\text{kcal mol}^{-1}$  [17]. Generally it is expected that diffusion along the cell boundary would be the rate-controlling step for cell growth [12].

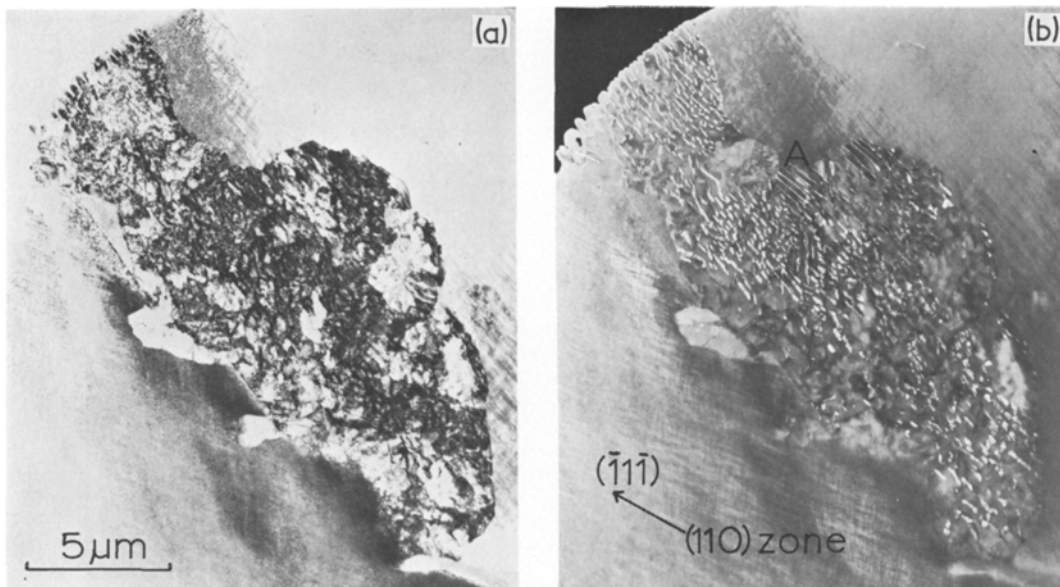


Figure 5 (a) Bright-field and (b) (100) $\gamma$  reflection dark-field electron micrographs of a typical colony of discontinuous precipitation reaction.

### 3.3. Transmission microscopy of discontinuous precipitation

Bright-field and dark-field micrographs of a discontinuous reaction cell are shown in Figs. 5a and b, respectively. The nickel phase is the continuous phase and has an orientation equivalent to the grain away from which it is growing as is typical of discontinuous precipitation [12]. The lamellar  $\gamma_{\text{NiBe}}$  phase has a simple cubic lattice with a lattice constant of  $2.61 \pm 0.02 \text{ \AA}$ . In general, the  $\gamma_{\text{NiBe}}$  phase has a very irregular morphology with no unique habit plane. However, in some regions, such as area A in Fig. 5b, the precipitate appears to have a clear crystallographic relationship with the nickel matrix. Diffraction results from several regions established a number of orientation relationships between the matrix and precipitate. The most frequently observed ones are listed in Table II. In any single cell all the  $\gamma_{\text{NiBe}}$  has a common orientation relationship to the matrix. However, one orientation is not common to all cells. In the copper–beryllium system several different closely oriented orientation relations have been suggested by various authors [7, 8].

TABLE II Observed discontinuous  $\alpha_{\text{Ni}}-\gamma_{\text{NiBe}}$  orientation relations

$(1\bar{1}0)_{\alpha_{\text{Ni}}}$	$\parallel$	$(120)_{\gamma_{\text{NiBe}}}$	$;$	$[110]_{\alpha_{\text{Ni}}}$	$\parallel$	$[001]_{\gamma_{\text{NiBe}}}$
$(001)_{\alpha_{\text{Ni}}}$	$\parallel$	$(100)_{\gamma_{\text{NiBe}}}$	$;$	$[110]_{\alpha_{\text{Ni}}}$	$\parallel$	$[001]_{\gamma_{\text{NiBe}}}$
$(1\bar{1}2)_{\alpha_{\text{Ni}}}$	$\parallel$	$(110)_{\gamma_{\text{NiBe}}}$	$;$	$[110]_{\alpha_{\text{Ni}}}$	$\parallel$	$[001]_{\gamma_{\text{NiBe}}}$

The interlamellar spacing for the alloy varied widely from colony to colony at the same ageing temperature. In fact, the range of spacings prevented quantitative determination of the temperature dependence of the interlamellar spacing. There was a qualitative trend toward larger spacings at higher temperatures but no quantitative measure could be obtained. Even samples of duplex aged samples showed no transition in spacing associated with the ageing temperature change. Apparently with some other parameters such as boundary misorientation dependence of the diffusion rate affects spacing more strongly than ageing temperature. Misorientation is known to affect strongly the rate of discontinuous phase growth [11].

### 3.4. Continuous precipitation

The continuous precipitation sequence for Ni–Be was analysed by a combination of selected area diffraction and dark-field microscopy. At  $650^\circ\text{C}$ , after ageing for five minutes, approximately 20% of the sample area transformed by the discontinuous reaction from grain boundaries.

Ageing for 5 min at  $650^\circ\text{C}$  produced the structure shown in Fig. 6. The narrow discontinuous precipitation region extends from a grain boundary. Motion of the cell boundary was arrested by a reaction of completely different morphology occurring in the remainder of the grain. The grain interior has undergone a continuous-type reaction to form

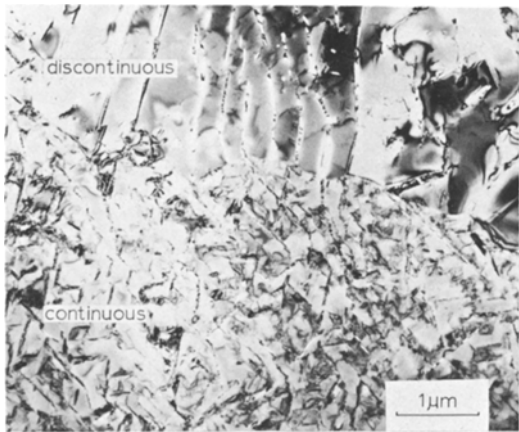


Figure 6 Electron micrograph showing boundary between discontinuous and continuous transformation regions of the stable  $\alpha + \gamma_{\text{NiBe}}$  phases.

a stable  $\gamma_{\text{NiBe}}$  directly from the  $\gamma'$  intermediate phase. Apparently the intermediate  $\gamma'$  phase coarsens rapidly enough at  $650^\circ\text{C}$  and above so that the driving force for the discontinuous reaction is eliminated. The driving force for discontinuous

reactions has been reviewed in detail by Hornbogen [18]. In copper–beryllium, only the discontinuous reaction is seen for all temperatures [8].

The diffraction pattern in Fig. 7a can be used to analyse the precipitate–matrix orientation relationship. The pattern is a  $[1\ 1\ 0]_{\alpha_{\text{Ni}}}$  zone axis matrix pattern with two variants of the  $[1\ 0\ 0]_{\gamma_{\text{NiBe}}}$  zone axis. The  $(1\ 0\ 0)$  reflections in the two  $[0\ 0\ 1]_{\gamma_{\text{NiBe}}}$  zones are rotated about  $6.5^\circ$  from the  $(0\ 0\ 2)_{\alpha_{\text{Ni}}}$ . The orientation relation that describes this pattern is  $(1\ 1\ 3)_{\alpha_{\text{Ni}}} \parallel (1\ 3\ 0)_{\gamma_{\text{NiBe}}}$ :  $[1\ \bar{1}\ 0]_{\alpha_{\text{Ni}}} \parallel [0\ 0\ 1]_{\gamma_{\text{NiBe}}}$ . This relation has been proposed by Bonfield for copper–beryllium as an intermediate state orientation before the final equilibrium transformation to  $(\bar{1}\ 1\ 1)_{\alpha_{\text{Cu}}} \parallel (\bar{1}\ 1\ 0)_{\gamma_{\text{CuBe}}}$ :  $[1\ 1\ 0]_{\alpha_{\text{Cu}}} \parallel [0\ 0\ 1]_{\gamma_{\text{CuBe}}}$  [8].

The habit plane of the  $\gamma_{\text{NiBe}}$  platelets formed by the continuous reaction can be deduced from the micrographs and diffraction patterns of Fig. 7. The two micrographs from  $(1\ 0\ 0)_{\gamma_{\text{NiBe}}}$  reflections

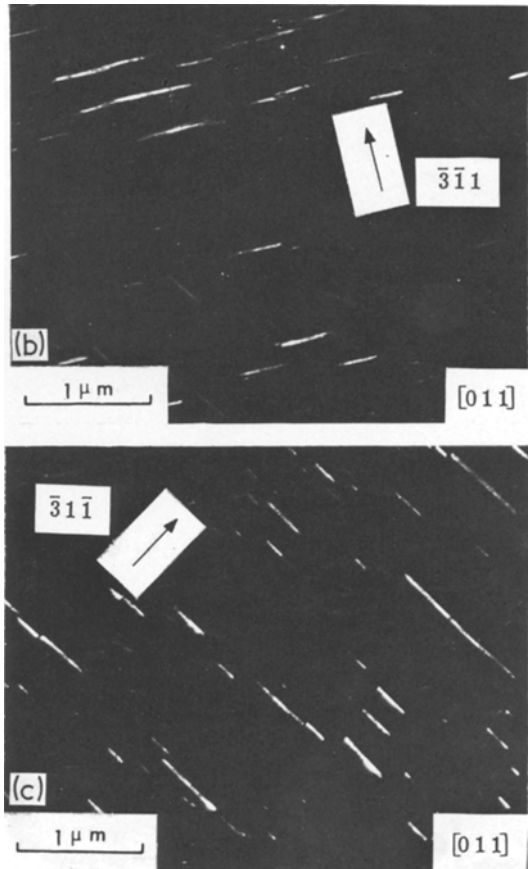
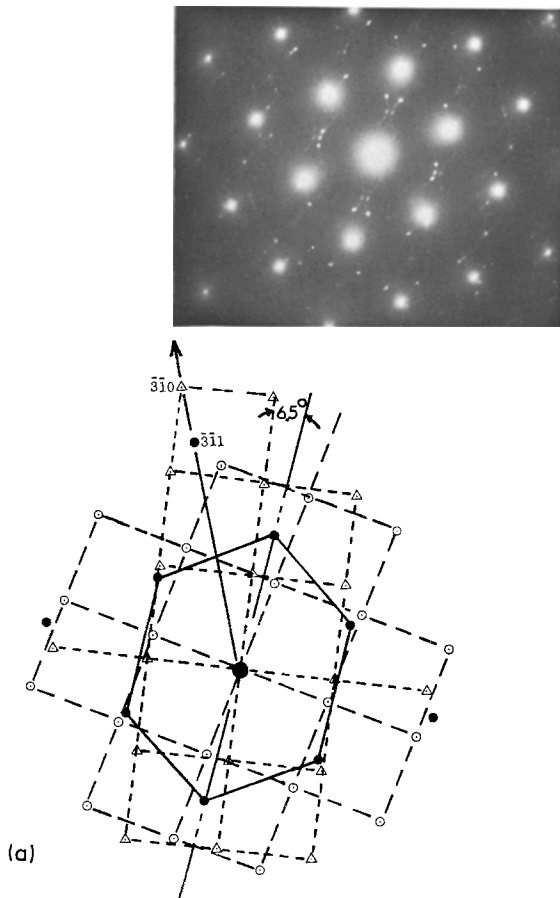
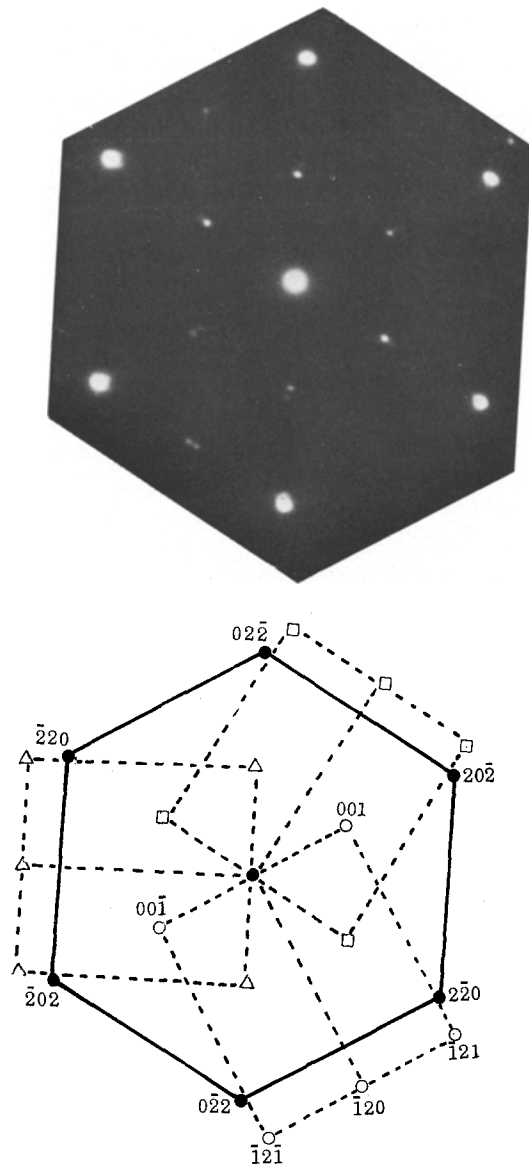


Figure 7 Series of electron micrographs giving diffraction pattern (a) and two variants of  $(0\ 0\ 1)_{\gamma_{\text{NiBe}}}$  reflection (b) and (c) dark-field images for continuous precipitation reaction.



(a)

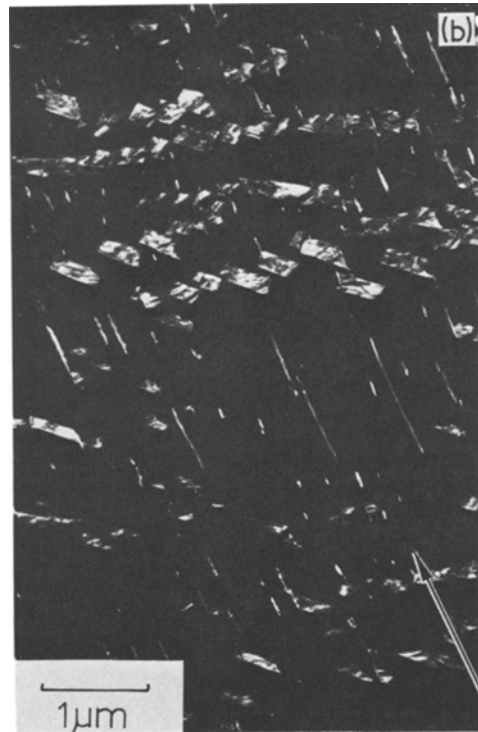


Figure 8 Series of electron micrographs giving the  $[111]_{\alpha\text{Ni}}$  diffraction pattern (a) and three variants of  $(100)_{\gamma\text{NiBe}}$  dark-field reflections for continuous precipitation reaction.

(Figs. 7b and c) show two variants of the precipitate plates sharply inclined or normal to the foil surface. Measurement of the angle between the surface traces of these planes yields a value of  $\sim 51^\circ$ . For the  $[110]$  matrix zone axis, two  $\{113\}$  matrix planes lie normal to the surface with a  $50.9^\circ$  interplanar angle. This suggests the habit plane is of the type  $\{113\}$ .

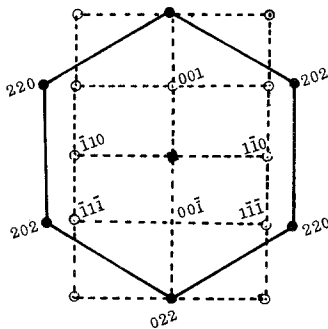
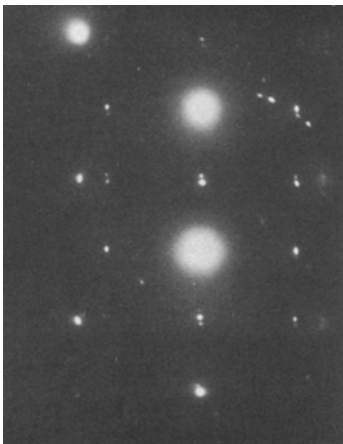
Dark-field on  $\{100\}$  precipitate reflections for the  $[111]$  matrix zone axis gives three variants

sharply inclined with  $60^\circ$  angles between the traces, as shown in Fig. 8. This result also fits with a  $\{113\}$  habit plane. For copper–beryllium, the  $\{113\}$  habit plane was proposed for the  $\gamma_{\text{CuBe}}$  discontinuous reaction [8].

Other orientation relations are also observed. The dark-field analysis of the  $\gamma_{\text{NiBe}}$  reflections of Fig. 8 yields four variants of the precipitate phase. The sharply inclined precipitates shown in Figs. 8b, c and d correspond to three different  $[210]$  pre-



Figure 8 continued.



cipitate zones present as shown in the schematic of the diffraction pattern. This corresponds to the orientation relation  $(20\bar{2})_{\alpha\text{Ni}} \parallel (001)_{\gamma\text{NiBe}}$ :  $[111]_{\alpha\text{Ni}} \parallel [210]_{\gamma\text{NiBe}}$ . This is equivalent to the relation proposed by Geisler *et al.* [5] for  $\gamma_{\text{CuBe}}$ .

However, not all the platelets in Fig. 8b can be ascribed to this orientation relation. The platelets shown in Fig. 8b that are oriented nearly parallel to the foil surface appear only in the  $(100)_{\gamma\text{NiBe}}$  dark-field images and not the  $(120)_{\gamma\text{NiBe}}$  or  $(121)_{\gamma\text{NiBe}}$  spots corresponding to the orientation given previously. A tilt of about  $3^\circ$  about the tilt axis results in the diffraction pattern of Fig. 9. The platelets which are nearly parallel to the foil surface in Fig. 8b are in contrast for all  $\gamma_{\text{NiBe}}$  reflections of this pattern. Since the  $[111]$  matrix zone axis is present, a third possible orientation relation is possible:

$$(01\bar{1})_{\alpha\text{Ni}} \parallel (001)_{\gamma\text{NiBe}} : [111]_{\alpha\text{Ni}} \parallel [110]_{\gamma\text{NiBe}}$$

All of these orientation relations have been proposed for the equilibrium phase in copper–beryllium [5, 8].

Figure 9 Diffraction pattern for a  $3^\circ$  tilt about  $(0\bar{2}2)_{\alpha}$  tilt axis shown in Fig. 8a. Platelets parallel to surface in Fig. 8b are in contrast for all  $\gamma_{\text{NiBe}}$  reflections.



The total angular difference between the three observed orientation relationships is only  $3^{\circ} 56'$ . From the present result, it is apparent that an unequivocal selection between the three relations is not possible using conventional selected area diffraction and dark-field microscopy. This technique was used in the present study and the earlier studies on copper–beryllium. Either selected area diffraction lacks sufficient resolution or the precipitate does vary slightly for different variants of the habit plane. A similar conclusion can probably be drawn about the disagreement in the copper–beryllium results.

#### 4. Conclusions

(1) The intermediate precipitation sequence is identical to copper–beryllium:  $\alpha$  (supersaturated solid solution)  $\rightarrow \alpha + \text{GP zones} \rightarrow \alpha + \gamma'_{\text{NiBe}} \rightarrow \alpha + \gamma_{\text{NiBe}}$

(2) For ageing temperatures up to  $565^{\circ}\text{C}$ , nickel–beryllium transformed to the equilibrium phase by a discontinuous reaction analogous to the copper–beryllium system.

(3) The kinetics of the reaction follow a linear growth rate as is common for discontinuous type reactions.

(4) The activation energy of  $58 \pm 3 \text{ kcal mol}^{-1}$  is well above that for grain boundary diffusion of nickel in nickel but below that for bulk diffusion. Alloying is known to reduce grain boundary diffusion rates in nickel.

(5) The orientation relation of the discontinuous precipitate varies from cell to cell with the most common being  $(001)_{\alpha\text{Ni}} \parallel (100)_{\gamma\text{NiBe}} : [110]_{\alpha\text{Ni}} \parallel [001]_{\gamma\text{NiBe}}$ . There is no unique habit plane.

(6) At  $650^{\circ}\text{C}$  and above the discontinuous reaction is stopped by the  $\gamma'$  intermediate particles transforming directly to  $\gamma$ .

(7) For continuous  $\gamma_{\text{NiBe}}$ , three closely oriented orientation relations were found that correspond to the three proposed for copper–beryllium. All were found for the same ageing time and temperature. Either all three are uniquely present or the accuracy level of selected area diffraction is such

that the small differences in orientation cannot be distinguished. The habit plane was  $\{113\}$ .

#### Acknowledgements

The assistance of W. J. Koone throughout the experimental work is acknowledged. M. R. Gutierrez prepared the metallographic samples and K. E. Lawson performed the areal fraction measurements. The critical review of the manuscript by T. J. Headley and K. H. Eckelmeyer is acknowledged.

#### References

1. HANS-GUNTER BAER and I. PFEIFFER, *Z. Metallk.* **63** (1972) 740.
2. A. GUINNER and P. JACQUET, *Rev. Met.* **41** (1944) 1.
3. R. J. PRICE and A. KELLY, *Acta. Met.* **11** (1963) 915.
4. I. PFEIFFER, *Z. Metallk.* **56** (1965) 465.
5. A. H. GEISLER, J. H. MALLERY and F. E. STEIGERT, *Trans. Met. Soc. AIME* **194** (1952) 307.
6. L. E. TANNER, *Phil. Mag.* **14** (1966) 111.
7. S. YAMAMOTO, M. MATSUI and Y. MURUKAMI, *Trans. Japan Inst. Met.* **12** (1971) 159.
8. W. BONFIELD and B. C. EDWARDS, *J. Mater. Sci.* **9** (1974) 398.
9. E. HORNBOGEN and M. ROTH, *Z. Metallk.* **58** (1967) 842.
10. W. GRUHL and D. AMMAN, *Acta. Met.* **3** (1955) 347.
11. J. W. CAHN, *ibid.* **4** (1956) 217.
12. C. S. SMITH, *ASM Trans. Quart.* **45** (1953) 533.
13. G. MEYRICK and G. W. POWELL, *Ann. Rev. Mater. Sci.* **3** (1973) 340.
14. W. BONFIELD and B. C. EDWARDS, *J. Mater. Sci.* **9** (1974) 409.
15. R. HOFFMAN, F. PICKUS and R. WARD, *Trans. AIME* **206** (1956) 483.
16. W. R. UPTHEGROVE and M. J. SIRROT, *Trans. ASM* **50** (1958) 1031.
17. M. A. GUBERCVA and L. M. MORO, "Diffusion Processes, Structure and Properties of Metals," edited by S. Z. Bokstein (Consultants Bureau, New York, 1965) p. 9.
18. E. HORNBOGEN, *Met. Trans.* **3** (1972) 2717.

Received 10 October and accepted 14 December 1977.